First-principles study of the magnetic and electronic properties of K-coated FeSe films

Xiao-Xiao Man,[1] Jian-Feng Zhang,[2] Pei-Han Sun,[3] Huan-Cheng Yang,[1,4] Zhong-Yi Lu,[1,4,*] and Kai Liu[1,4,†]

[1]*Department of Physics and Beijing Key Laboratory of Opto-electronic Functional Materials & Micro-nano Devices, Renmin University of China, Beijing 100872, China*

[2]*Institute of Physics, Chinese Academy of Sciences, Beijing 100190, China*

[3]*School of Science, Hebei University of Science and Technology, Shijiazhuang, Hebei 050018, China*

[4]*Key Laboratory of Quantum State Construction and Manipulation (Ministry of Education), Renmin University of China, Beijing 100872, China*

(Received 5 September 2023; revised 15 November 2023; accepted 11 December 2023; published 3 January 2024)

Recent experiments have reported that depositing K atoms onto the surfaces of nonsuperconducting FeSe thin films can not only transform them into superconductors but also obtain a domelike relation between the superconducting transition temperature (T_c) and the K coverage (K_c). To elucidate the mechanism underlying the domelike dependence of T_c on K_c in K-coated FeSe (K/FeSe) films, we have studied the electronic and magnetic properties of the K/FeSe films at $K_c = 0.125$, 0.25, and 0.5 ML [1 monolayer (ML) is defined as the areal density of the topmost Se site] based on the first-principles electronic structure calculations. Our calculations show that there are two antiferromagnetic (AFM) states being energetically quite close to each other regardless of the value of K_c, indicating that there may exist strong magnetic fluctuations in K/FeSe. On the other hand, it is worth noting that the differential charge and spin densities between the two AFM states at three K_c's demonstrate that both the charge density redistributions around Se atoms and the spin density redistributions around Fe atoms have the domelike evolution with K_c, which coincide with the observed behavior of superconducting T_c. Furthermore, we find that the densities of states at the Fermi level [$N(E_F)$] in these two AFM states also have a domelike dependence on K_c. Apart from helping us understand the superconducting mechanism in the K/FeSe system, these results also provide a different perspective for exploring the superconductivities in other FeSe-based superconductors.

DOI: 10.1103/PhysRevB.109.035105

I. INTRODUCTION

Iron-based superconductors have been one of the focuses in the condensed matter physics and the materials communities since their discoveries [1–7], yet the underlying superconducting (SC) mechanism is still under debate [8]. Among various iron-based superconductors, β-FeSe stands out as an ideal platform to explore the enigma of high-temperature superconductivity, partially due to its simplest crystal structure [1–7]. Interestingly, unlike the widely studied FeAs-based superconductors whose superconductivities often occur near the stripe antiferromagnetic (AFM) and nematic orders [9], FeSe only exhibits nematic order but no long-range AFM order at ambient pressure [10] and is already superconducting ($T_c \sim 8$ K) without tuning [2]. For iron pnictides, carrier doping is an effective approach to realize the high-T_c superconductivity, resulting in a domelike relation between the superconducting T_c and the doping density [9,11]. Similarly, for FeSe, there are also some means such as intercalation [12–21], chemical substitution [22], gate voltage [23], and epitaxial film growth [24] that have been utilized to dope carriers in FeSe to improve its superconducting T_c. The modulation of electronic and magnetic properties of the FeSe layers by carrier doping is believed to play an essential role in enhancing the superconductivity.

In 2015, Miyata *et al.* reported a strategy for the carrier doping of FeSe films, that is, depositing K atoms onto the surfaces of FeSe films [25]. By using this technique, the non-SC 3-unit-cell (3-UC)-thick FeSe film was successfully converted into a superconductor with T_c up to 48 K and its electronic phase diagram includes a SC dome [25]. This advance has greatly fueled the experimental and theoretical interests in the K-coated FeSe (K/FeSe) films [26–30]. Experimentally, *in situ* scanning tunneling spectroscopy (STM) measurements on the 1-UC- and 2-UC-thick K/FeSe films have revealed that the FeSe/$SrTiO_3$ (FeSe/STO) interface plays a vital role in enhancing the Cooper pairing in ultrathin FeSe films [26]. Subsequently, angle-resolved photoemission spectroscopy studies on 4-UC- to 50-UC-thick K/FeSe films have demonstrated that for the films thicker than 4 UC, the improved superconductivities are inherently related to the electron-doped top FeSe layer and are independent of the film thickness or the FeSe/STO interface [27], which is also evidenced by an STM experiment on a heavily K-doped FeSe multilayer film [28]. Moreover, the SC order parameter of the K/FeSe system, a key physical quantity to understand the high-T_c superconductivity, has been pointed out to be sign-reversal according to the quadratic low-temperature

*zlu@ruc.edu.cn
†kliu@ruc.edu.cn

variation in the London penetration depth [29]. Theoretically, a study combining density functional theory (DFT) and unfolding technique indicated that the experimentally observed Fermi-surface topology is caused by a strong electric field perpendicular to the FeSe film surface due to the charge transfer, which linearly depends on the K coverage (K_c) [30]. These studies have largely enriched our knowledge about the K/FeSe system from different perspectives. Nevertheless, the underlying reason for the experimentally observed domelike dependence of T_c on K_c in the K/FeSe system [25,27–29] is still an open question, which deserves in-depth theoretical investigation.

In this paper, we have systematically studied the evolution of the electronic and magnetic properties of the K/FeSe films with the K coverage K_c by using first-principles electronic structure calculations. We find that whether K_c is equal to 0.125, 0.25, or 0.5 monolayers (ML), there may be strong magnetic fluctuations between two AFM states in a narrow energy window. We further explored the variations of the differential charge and spin densities between the two AFM states along with K_c. Notably, the charge density redistributions around the Se atoms and the spin density redistributions around the Fe atoms both exhibit a domelike trend with increasing K_c, which are consistent with the experimental behavior of the superconducting T_c [29]. In addition, the electronic densities of states at the Fermi level in the two AFM states also possess the domelike relation with K_c. Beyond the generally recognized charge doping effect, our results provide a microscopic picture for the evolution of physical properties of the K/FeSe system with K coverage.

II. COMPUTATIONAL DETAILS

To study the atomic structure, electronic structure, and magnetic properties of 1-UC thick K/FeSe, fully spin-polarized DFT calculations were performed with the projector augmented wave method [31,32] as implemented in the VASP package [33–35]. The generalized gradient approximation of the Perdew-Burke-Ernzerhof type [36] was adopted for the exchange-correlation functional. After the convergence test, the kinetic energy cutoff of the plane-wave basis was chosen to be 480 eV. The in-plane lattice constants were set to the experimental values ($a = b = 3.773$ Å) of β-FeSe [37], and a vacuum layer larger than 15 Å was utilized to eliminate the interaction between the image slabs along the (001) direction. The DFT-D2 method [38,39] was used to account for the van der Waals interaction in the layered materials [40]. The $12 \times 12 \times 1$ and $3 \times 3 \times 1$ Monkhorst-Pack **k**-point meshes were adopted to sample the Brillouin zones (BZs) of the unit cell and the $2\sqrt{2} \times 2\sqrt{2}$ supercell of K/FeSe, respectively. The Gaussian smearing method with a width of 0.05 eV was used for the Fermi-surface broadening. The internal atomic positions were fully optimized until the residual forces on all atoms were smaller than 0.01 eV/Å. The energy convergence criterion was set to 10^{-6} eV. To study the magnetic properties of the FeSe layer, the nonmagnetic (NM) state, the ferromagnetic (FM) state, and four typical AFM states (single stripe, Néel, dimer1, and dimer2) were considered.

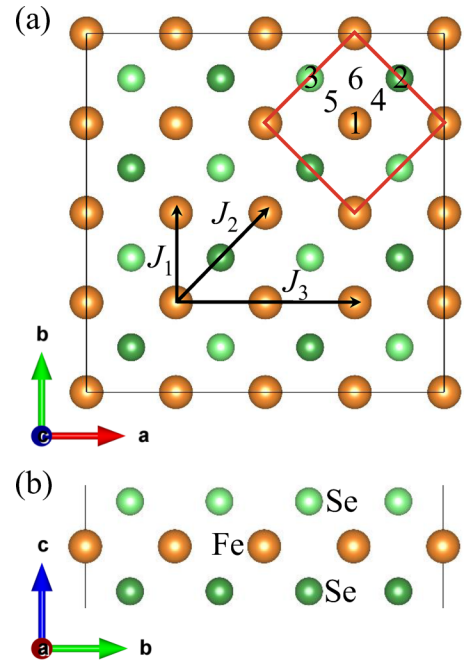

FIG. 1. (a) Top and (b) side views of the FeSe monolayer. The orange ball represents the Fe atom, while the light green and dark green balls distinguish the Se atoms above and below the Fe-Fe plane, respectively. The red and black squares in (a) outline the unit cell and the $2\sqrt{2} \times 2\sqrt{2}$ supercell, respectively. Six typical adsorption sites of the K atom on the FeSe layer are labeled by numbers 1–6 in (a). The exchange interactions between the Fe spins are also schematically shown in (a), including the nearest-neighboring (NN) exchange J_1, next-NN exchange J_2, and third neighboring exchange J_3.

III. RESULTS AND ANALYSIS

Figures 1(a) and 1(b) show the top and side views of monolayer FeSe, where Fe atoms form a squarelike plane sandwiched by two Se layers. The red and black squares in Fig. 1(a) represent the unit cell and the $2\sqrt{2} \times 2\sqrt{2}$ supercell, respectively. The exchange interactions between the Fe spins are also displayed in Fig. 1(a), which will be used in the following analyses on the magnetic couplings. In order to simulate the deposition of K atoms on the top layer of FeSe films, it is first necessary to find the most favorable adsorption site energetically for the K atom on monolayer FeSe, for which we considered six nonequivalent adsorption sites in the unit cell [Fig. 1(a)], including three top sites (labeled with 1, 2, and 3), two bridge sites (labeled with 4 and 5), and one hollow site (labeled with 6). The specific structures of 1-UC K/FeSe corresponding to the above adsorption sites are shown in Fig. 7 in the Appendix. According to our calculations, the energetically most stable one for the K atom is on the top of the Se atom below the Fe-Fe plane, as shown in Fig. 7(b) in the Appendix.

A previous experiment has demonstrated that when the thicknesses of FeSe epitaxial films exceed 4 UC, the enhanced superconductivities of FeSe films induced by K deposition are only related to the electron doping in the uppermost FeSe layer, being independent on the film thickness or the FeSe/STO interface [27]. In order to clarify how

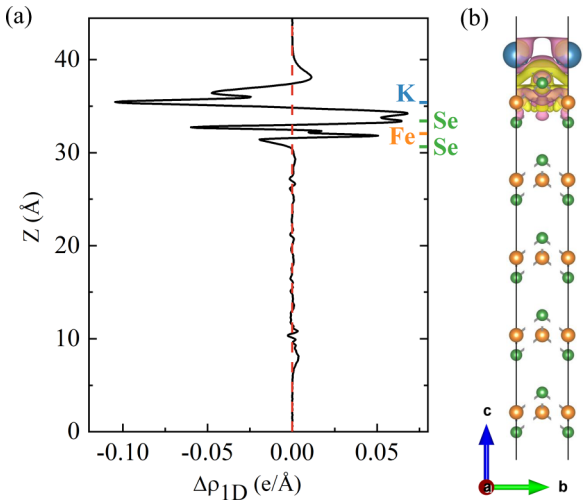

FIG. 2. (a) One-dimensional (1D) and (b) three-dimensional (3D) differential charge densities for the K-coated 5-UC FeSe films ($\Delta\rho = \rho_{\mathrm{K/FeSe}} - \rho_{\mathrm{FeSe}} - \rho_{\mathrm{K}}$). The atomic positions in (a) are marked by the color bars on the right axis. In (b), the dark blue, orange, and green balls represent the respective K, Fe, and Se atoms, while the yellow and pink isosurfaces represent the electron accumulation and depletion regions, respectively. The isosurface value is set to $6.5 \times 10^{-4}\ e/\text{Å}^3$.

the K adsorption affects the charge density redistributions in the FeSe layers, we calculated the one-dimensional (1D) and three-dimensional (3D) differential charge densities for 5-UC K/FeSe [Figs. 2(a) and 2(b)], so as to determine the number of FeSe layer used in our calculations. It can be seen clearly that, consistent with previous experiments [27,41], the calculated charge density redistribution is the most significant for the FeSe layer closest to the K atoms. So we will use 1-UC K/FeSe in the following calculations. In this way, not only can the computational consumption be reduced, but also the effect of K deposition on the physical properties of the topmost FeSe layer can be reasonably simulated.

In order to understand the domelike (T_c, K_c) phase diagram of K/FeSe in the previous experiment [29], we next used the 1-UC K/FeSe model determined above and selected three K_c's ($K_c = 0.125$, 0.25, and 0.5 ML) to investigate the evolution of the electronic and magnetic properties of the topmost FeSe layer with the K coverage (electron doping). Here, 1 ML is defined as the areal density of the topmost Se site [28,29]. After determining the adsorption positions of the K atoms for three K_c's as in Fig. 8 of the Appendix, we first studied the magnetic properties of 1-UC K/FeSe at $K_c = 0.125$, 0.25, and 0.5 ML. Figure 3 schematically displays the spin configurations of the single-stripe AFM, checkboard AFM Néel, dimer1 AFM, and dimer2 AFM states at three K_c's. The difference between the dimer1 and dimer2 AFM states is that their local spin patterns around each K atom are different (Fig. 3). The calculated relative energies of these magnetic states with respect to that of the NM state in each K_c are listed in Table I. Obviously, regardless of the value of K_c, the sequence among these magnetic states from low energy to high energy is E_{dimer1}, E_{dimer2}, $E_{\mathrm{single\text{-}stripe}}$, $E_{\mathrm{Néel}}$,

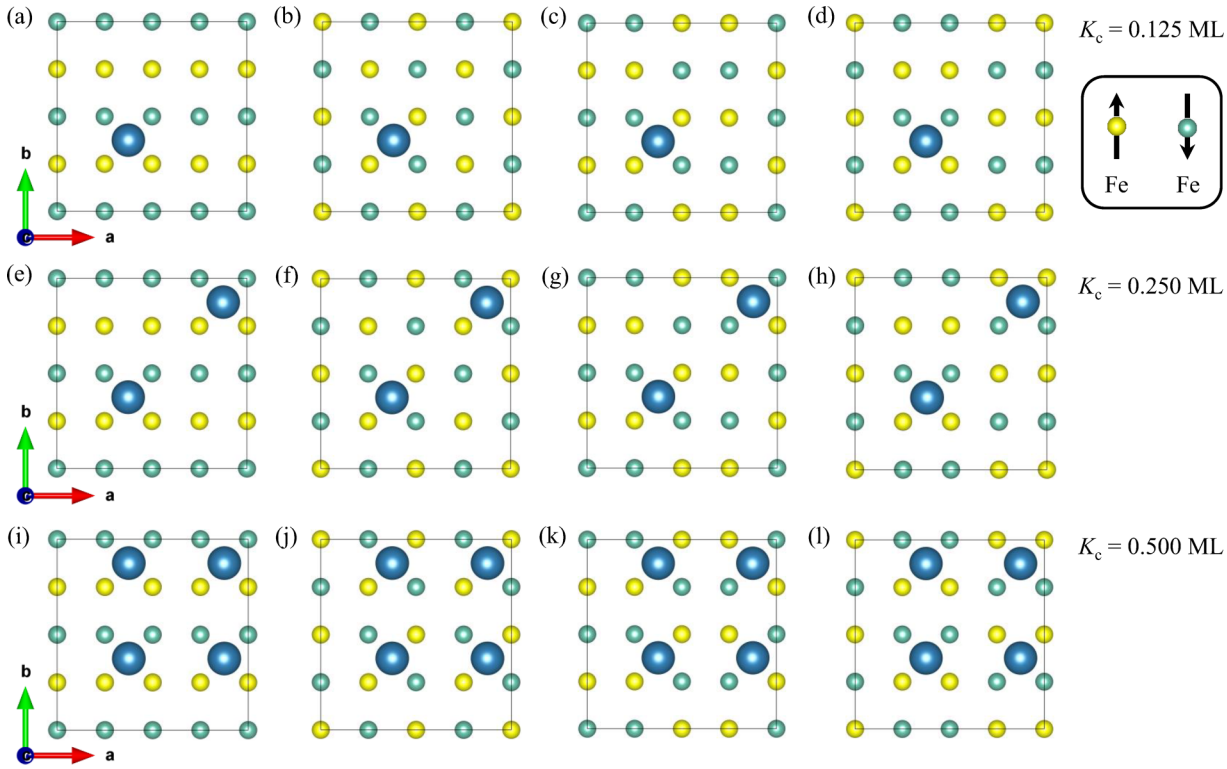

FIG. 3. Sketches of four typical spin configurations for the Fe lattice in 1-UC K/FeSe at $K_c = 0.125$, 0.25, and 0.5 ML. (a), (e), and (i) Single-stripe AFM state. (b), (f), and (j) Checkerboard AFM Néel state. (c), (g), and (k) Dimer1 AFM state. (d), (h), and (l) Dimer2 AFM state. Here, the solid square represents the $2\sqrt{2} \times 2\sqrt{2}$ supercell, while the dark blue, yellow, and green balls represent the K atoms, spin-up Fe atoms, and spin-down Fe atoms, respectively.

TABLE I. Relative energies ΔE (in units of meV/Fe) of the single-stripe AFM, checkerboard AFM Néel, dimer1 AFM, and dimer2 AFM states with respect to the NM state for 1-UC K/FeSe at $K_c = 0.125$, 0.25, and 0.5 ML. The corresponding average local moments $\overline{M}$ (in units of μ_B) on Fe atoms are also listed.

State	$K_c = 0.125$		$K_c = 0.250$		$K_c = 0.500$	
	ΔE	$\overline{M}$	ΔE	$\overline{M}$	ΔE	$\overline{M}$
NM	0.00		0.00		0.00	
Single stripe	−78.38	2.15	−76.49	2.15	−81.82	2.20
Néel	−59.92	1.85	−62.41	1.85	−59.34	1.75
Dimer1	−93.20	2.05	−91.52	2.05	−88.55	2.05
Dimer2	−93.00	2.10	−90.14	2.05	−84.59	2.00

and E_{NM}. In addition, it is worth noting that the energy of the dimer1 AFM state is always lower than but very close to that of the dimer2 AFM state, with the energy differences being 0.20, 1.38, and 3.96 meV/Fe when $K_c = 0.125$, 0.25, and 0.5 ML, respectively. It turns out that there may exist magnetic fluctuations between the dimer1 and dimer2 AFM states in a narrow energy window at three K_c's. However, the energy window exhibits a monotonic increase when K_c changes from 0.125 to 0.25 then to 0.5 ML, which is inconsistent with the experimental domelike relationship between T_c and K_c [29].

We next study the differential charge and spin densities between the dimer1 and dimer2 AFM states at $K_c = 0.125$, 0.25, and 0.5 ML. The differential charge densities between the two dimer AFM states at three K_c's are shown in Figs. 4(a)–4(c). Visually, when K_c varies from 0.125 to 0.25 then to 0.5 ML, the volumes of the charge redistribution regions around the Se atoms first increase and then decrease, while those of the Fe atoms change slightly but show a similar tendency. In addition, it is interesting that the charge density redistributions around the Se atoms along the c axis at each K_c are analogous to the electric dipoles. To quantitatively see how the charge redistributions around the Se atoms vary with K_c, we plotted the z-directional 1D differential charge densities between the two dimer AFM states for some representative Se atoms [Se1, Se2, and Se3 in Fig. 4(b)] at each K_c, which are displayed in Figs. 5(a)–5(c), respectively. Notably, the 1D differential charge densities of the three Se atoms all reach maximum values at $K_c = 0.25$ ML, and are all lower at $K_c = 0.125$ and 0.5 ML, being in line with the experimentally observed domelike variation of superconducting T_c with K_c [29].

Now we discuss the differential spin densities between the two dimer AFM states at three K_c's [Figs. 4(d)–4(f)]. Obviously, for the Se atoms, the volumes of the spin density redistribution regions barely change when K_c varies, so we mainly focus on those around the Fe atoms. As seen from Figs. 4(d)–4(f), the spin density redistributions around the Fe atoms in the first, third, and fifth columns are much more dramatic than those in the second and fourth columns. The reason is that the spin polarizations of the Fe atoms in the former three columns of the dimer1 AFM state [Figs. 3(c), 3(g), and 3(k)] are all exactly opposite to those of the dimer2 AFM state [Figs. 3(d), 3(h), and 3(l)], while the spin polarizations of Fe atoms in the latter two columns are all the same in the two dimer AFM states. On the other hand, it is noticeable that the volumes of the spin density redistribution regions around the second and fourth column Fe atoms also increase when K_c varies from 0.125 to 0.25 ML and then decrease from 0.25 to 0.5 ML, which agree well with the domelike relationship between superconducting T_c and K_c [29]. The same conclusion can be drawn from the (100) planar two-dimensional (2D) differential spin densities [as displayed in Figs. 5(d)–5(f)] between the two dimer AFM states for the Fe atoms in the second column [dashed line in Fig. 4(f)]. Since the p electrons of Se atoms can bridge the magnetic exchange interactions

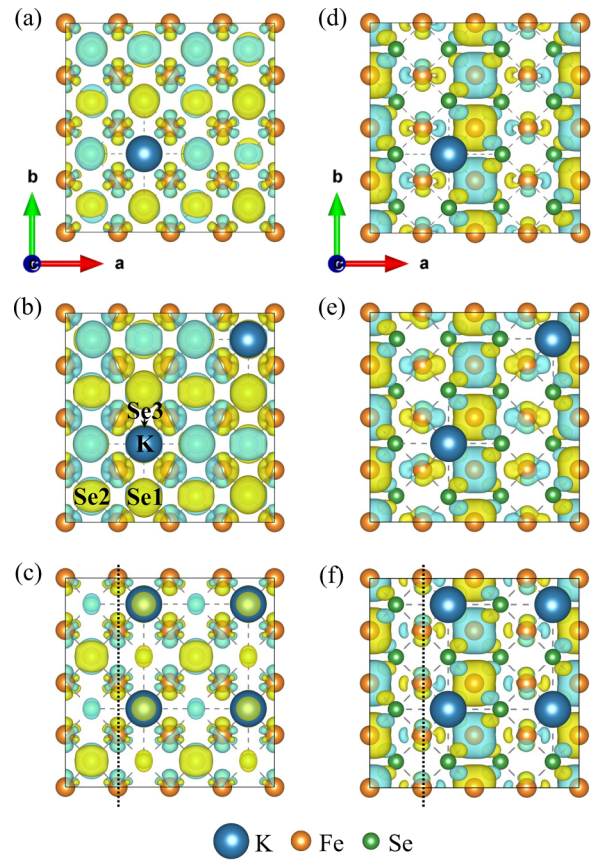

FIG. 4. (a)–(c) Differential charge densities with an isosurface value of 0.0035 $e/Å^3$ between the dimer1 and dimer2 AFM states of 1-UC K/FeSe at $K_c = 0.125$, 0.25, and 0.5 ML, respectively. (d)–(f) Differential spin densities with an isosurface value of 0.005 $e/Å^3$ between the dimer1 and dimer2 AFM states of 1-UC K/FeSe at $K_c = 0.125$, 0.25, and 0.5 ML, respectively. The dark blue, orange, and green balls represent the K, Fe, and Se atoms, respectively. The yellow and sky blue isosurfaces represent the electron accumulation and depletion regions, respectively.

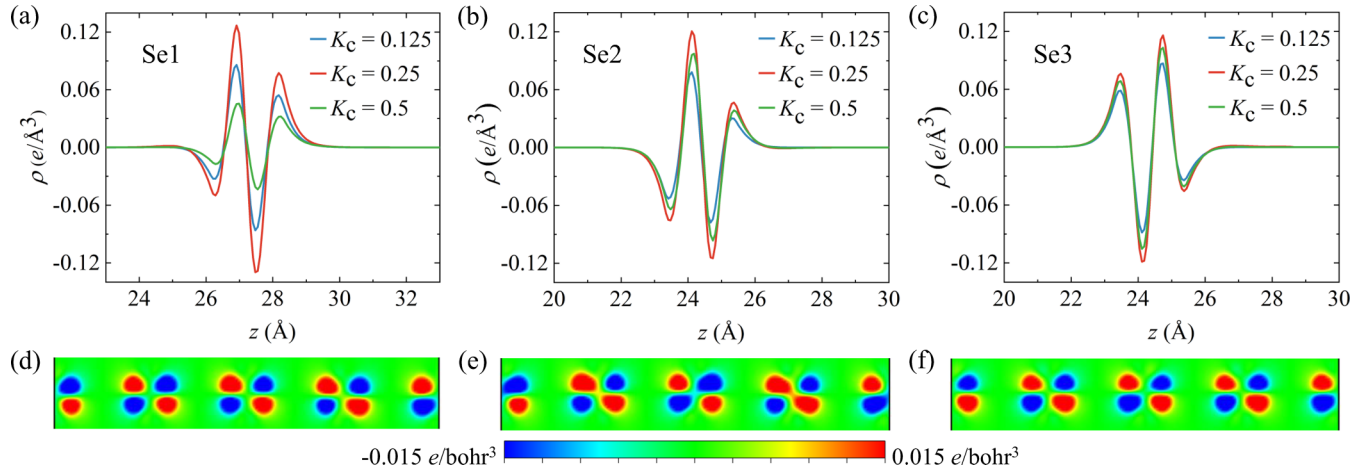

FIG. 5. (a)–(c) The z-directional 1D differential charge densities between the dimer1 and dimer2 AFM states near Se1, Se2, and Se3 atoms, respectively. The Se1, Se2, and Se3 atoms are labeled in Fig. 4(b), where the Se1 (Se2/3) atom is located above (below) the Fe plane. Here, it should be noted that the Se3 atom is covered by the K atom above it in the top view [Fig. 4(b)]. The blue, red, and green curves correspond to those at $K_c = 0.125$, 0.25, and 0.5 ML, respectively. (d)–(f) The (100) planar two-dimensional (2D) differential spin densities between the dimer1 and dimer2 AFM states across the Fe atoms marked by the vertical dotted line in Fig. 4(f) at $K_c = 0.125$, 0.25, and 0.5 ML, respectively. The maximum and minimum values on the color bar are set to 0.015 and -0.015 e/bohr^3, respectively.

between the Fe spins, hence when K_c increases from 0.125 to 0.25 then to 0.5 ML, the consistency between the nonmonotonic changes of the charge density redistributions around the Se atoms and the spin density redistributions around the Fe atoms indicates that the mutual coupling between the charge and spin degrees of freedom may have a close relationship with the experimental domelike variation of superconducting T_c with increasing K_c in K/FeSe [29].

The density of states (DOS) at the Fermi level, $N(E_F)$, is also one of the factors affecting the superconducting T_c of a superconductor [42]. Specifically, increasing $N(E_F)$ in a conventional superconductor can enhance its T_c to some extent. Even for an unconventional superconductor, $N(E_F)$ could affect the itinerant carriers that mediate the magnetic interactions [43] and the superconducting T_c [44–46]. Here, for the K/FeSe system, we calculated the total DOSs of 1-UC K/FeSe in the lowest-energy dimer1 AFM state at $K_c =$ 0.125, 0.25, and 0.5 ML [Figs. 6(a)–6(c)] and displayed the

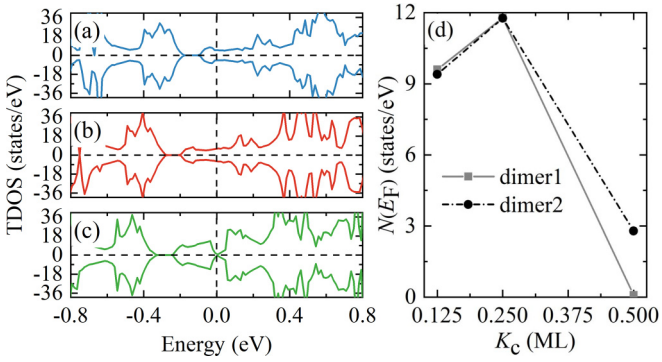

FIG. 6. (a)–(c) The total DOS for 1-UC K/FeSe in the dimer1 AFM state at $K_c = 0.125$, 0.25, and 0.5 ML, respectively. (d) The calculated evolution of DOS at the Fermi level $N(E_F)$ with K_c for 1-UC K/FeSe. Here, the gray squares and black dots represent the $N(E_F)$ values obtained in the dimer1 and dimer2 AFM states, respectively.

corresponding evolution of $N(E_F)$ with K_c in Fig. 6(d). As seen from Figs. 6(a)–6(c), the Fermi level naturally moves up with an increase of K_c because more electrons are transferred from the K atoms to the FeSe layer. Remarkably, $N(E_F)$ in the dimer1 AFM state counts on K_c domelikely, as shown by the gray solid line in Fig. 6(d). Similarly, the black dotted line in Fig. 6(d) shows that $N(E_F)$ in the dimer2 AFM state has the same dependence on K_c. The evolution trend of $N(E_F)$ with K_c is thus also consistent with the domelike relationship between T_c and K_c of K/FeSe [29].

IV. DISCUSSION AND SUMMARY

To understand the underlying reasons for the energy sequence among various magnetic states in 1-UC K/FeSe, we calculated the exchange interactions among the Fe spins at $K_c = 0.125$, 0.25, and 0.5 ML by employing an effective Heisenberg model,

$$H = J_1 \sum_{\langle i,j \rangle} \vec{S}_i \cdot \vec{S}_j + J_2 \sum_{\langle\langle i,j \rangle\rangle} \vec{S}_i \cdot \vec{S}_j + J_3 \sum_{\langle\langle\langle i,j \rangle\rangle\rangle} \vec{S}_i \cdot \vec{S}_j,$$

where J_1, J_2, and J_3 denote the respective couplings between the nearest, the next-nearest, and the third-nearest neighboring Fe spins [Fig. 1(a)], and S is the local magnetic moment on the Fe atom. According to above model, the dimer1 and dimer2 AFM states have the same energy formula, so the calculated energies of the two are all quite close at each K_c (Table I). In addition, the dimer (single-stripe) AFM state will have a lower energy than the single-stripe (Néel) AFM state once the couplings fulfill the conditions $J_1 > 2J_2 - 2J_3$ ($2J_2 > J_1$). From our calculated energy differences among the magnetic states of 1-UC K/FeSe at each K_c (Table I), we obtain the corresponding values of J_1, J_2, and J_3 displayed in Table II, which naturally explains the energy sequence among the dimer, single-stripe, and Néel AFM states.

In FeSe-based superconductors, there are couplings among multiple degrees of freedom, such as charge, spin, orbital,

TABLE II. Exchange couplings J_1, J_2, and J_3 (in units of meV/S^2) between the Fe spins for 1-UC K/FeSe at $K_c = 0.125$, 0.25, and 0.5 ML calculated via the energy differences among the single-stripe AFM, checkerboard AFM Néel, dimer1 AFM, and bicollinear AFM states.

K_c	J_1	J_2	J_3
0.125	49.1	26.9	6.0
0.250	42.0	22.7	5.5
0.500	23.5	14.5	4.5

and lattice. The explorations of the superconducting mechanism of FeSe-based superconductors are exactly based on these degrees of freedom and their couplings. Taking the FeSe/STO film as an example, some studies focusing on the charge degree of freedom have shown the important role of charge transfer from STO to FeSe in improving the superconductivity [47–52]. Others discussing the spin degree of freedom have suggested that superconductivity appears when the spin density waves in FeSe film are suppressed [53]. Those concentrating on the couplings among charge, lattice, and spin degrees of freedom have indicated that the coupling between FeSe electrons and STO phonons can enhance the spin fluctuations and thus the superconducting T_c [54–58]. In addition, other work considering the orbital degree of freedom has revealed that orbital fluctuation has a negligible effect on Cooper pairing in iron-based superconductors [59]. Here, our theoretical studies on the K/FeSe system pay attention to the coupling between the charge and spin degrees of freedom. On the one hand, there may exist spin fluctuations between the dimer1 and dimer2 AFM states in a narrow energy window at each K_c according to Table I. However, the energy window increases monotonically when K_c varies from 0.125 to 0.25 then to 0.5 ML, which is different from the domelike relationship between T_c and K_c [29]. Therefore, we suggest that merely the spin fluctuations may be not enough to explain the superconductivity in the K/FeSe system. On the other hand, the domelike dependence of the electronic DOS $N(E_F)$ on K_c in the two dimer AFM states [Fig. 6(d)] indicates that the density of itinerant carriers at the Fermi level may play a partial role in the Cooper pairing. Notably, our results about the domelike variations of differential charge densities and differential spin densities between the two dimer AFM states along with the K_c, which is similar to the behavior of superconducting T_c, demonstrate that the coupling between charge and spin degrees of freedom is conductive to the superconductivity in the K/FeSe system (Figs. 4 and 5). Last but not least, our calculated (100) planar 2D differential charge and spin densities between the two dimer AFM states show that the charge and spin density redistributions around the Fe atoms possess the characteristics of electric and magnetic quadrupoles (Figs. 9 and 5) [60], respectively. Meanwhile, we noted that recent studies on unconventional superconducting mechanism have extended to multipole-fluctuation-mediated superconductivity [61–64]. As for whether multipole fluctuations exist in the K/FeSe system, and if so, whether they are related to superconductivity, further explorations are needed. These above results thus provide helpful references for the further studies on the superconducting mechanism of the K/FeSe system.

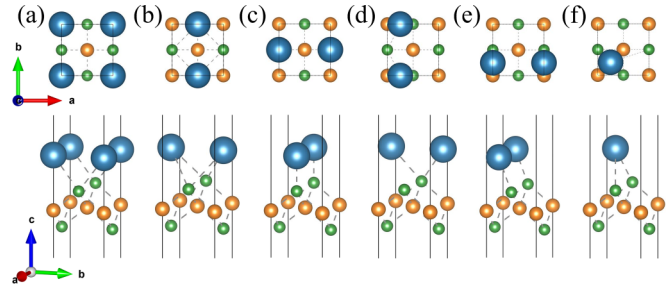

FIG. 7. Six typical atomic structures of 1-UC K/FeSe, while one K atom adsorbs in the unit cell of monolayer FeSe. In each panel, the upper (bottom) part displays the top (side) view. The dark blue, orange, and green balls represent the K, Fe, and Se atoms, respectively.

In summary, we have investigated the electronic and magnetic properties of 1-UC K/FeSe at $K_c = 0.125$, 0.25, and 0.5 ML via first-principles electronic structure calculations. Our calculations show that regardless of whether $K_c = 0.125$ or 0.25 or 0.5 ML, there may exist strong AFM fluctuations between the dimer1 and dimer2 AFM states in a narrow energy window, which increases from 0.20 to 1.38 then to 3.96 meV/Fe with K_c. It is worth noting that the charge (spin) density redistributions around the Se (Fe) atoms between the two low-energy dimer AFM states and the density of states at the Fermi level [$N(E_F)$] in the two dimer AFM states all show the domelike dependence on K_c, which may be intimately related to previous experimental observation on the domelike evolution of superconducting T_c with K_c in 2.5-UC K/FeSe [29]. Our work provides a microscopic picture about the variation of the electronic and magnetic properties in the low-energy states of K/FeSe with the K doping, which may facilitate the comprehensive understanding of the superconductivity in the K/FeSe system as well as the related FeSe-based superconductors.

ACKNOWLEDGMENTS

This work was supported by the National Natural Science Foundation of China (Grants No. 12174443 and No. 11934020), the National Key R&D Program of China (Grants No. 2022YFA1403103, No. 2019YFA0308603, and No. 2017YFA0302903), and the Beijing Natural Science Foundation (Grant No. Z200005). Computational resources were provided by the Physical Laboratory of High Performance Computing at Renmin University of China and the Beijing Super Cloud Computing Center.

APPENDIX

Figures 7(a)–7(f) show the atomic structures of 1-UC K/FeSe corresponding to six typical adsorption sites of a K atom on a FeSe monolayer shown in Fig. 1(a), respectively. After relaxing these structures in the NM state, we found that the energetically most stable one is that displayed in Fig. 7(b), where the K atom is located on the top of the bottom Se atom below the Fe-Fe plane.

When the K atom coverage on the FeSe layer is less than 1 ML, the relative position between the K atoms should be con-

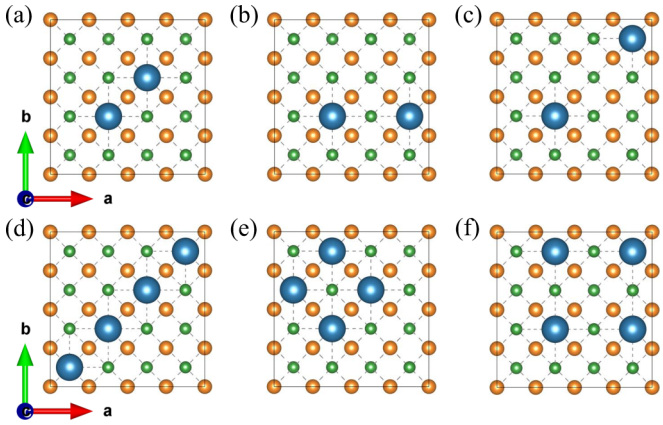

FIG. 8. (a)–(c) Three typical atomic structures of 0.25-ML K coverage on FeSe, while two K atoms adsorb in the $2\sqrt{2} \times 2\sqrt{2}$ supercell of monolayer FeSe. (d)–(f) Three typical atomic structures of 0.5-ML K coverage on FeSe, while four K atoms adsorb in the $2\sqrt{2} \times 2\sqrt{2}$ supercell of monolayer FeSe. The dark blue, orange, and green balls represent the K, Fe, and Se atoms, respectively.

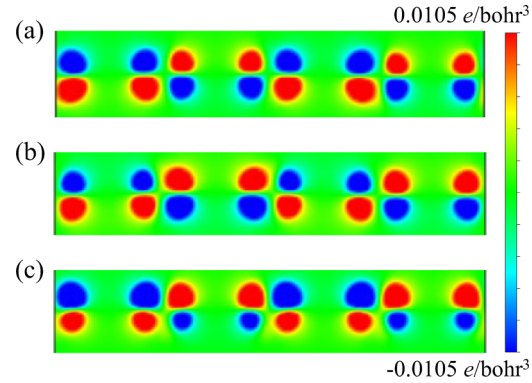

FIG. 9. (a)–(c) The (100) planar 2D differential charge densities between the dimer1 and dimer2 AFM states across the Fe atoms marked by the vertical dotted line in Fig. 4(c) at $K_c = 0.125$, 0.25, and 0.5 ML, respectively. The maximum and minimum values on the color bar are set to 0.0105 and $-0.0105\ e/\text{bohr}^3$, respectively.

sidered. In a $2\sqrt{2} \times 2\sqrt{2}$ supercell of monolayer FeSe that we used in the calculations, the distances between two K atoms can be a, $\sqrt{2}a$, or $2a$ when $K_c = 0.25$ ML, which are shown in Figs. 8(a)–8(c), respectively. After structural optimization, it is found that the one shown in Fig. 8(c) possesses the lowest energy. For K_c of 0.5 ML, there were also three typical structures in the same supercell considered when four K atoms are adsorbed [Figs. 8(d)–8(f)], among which the one displayed in Fig. 8(f) is the most stable. Clearly, whether two or four K atoms adsorb on the FeSe layer, the most energetically favorable structures have the same characteristic, that is, the distances between the adsorbed K atoms should be as far as possible.

Figures 9(a)–9(c) display the (100) planar 2D differential charge densities between the dimer1 and dimer2 AFM states for the Fe atoms in the second column [dashed line in Fig. 4(c)] at three K_c's. It is found that the charge density redistributions around the Fe atoms all show the characteristics of electric quadrupole at three K_c's, as schematically shown in a previous report [60]. Similarly, the magnetic quadrupole features can also be seen from the (100) planar 2D spin density redistributions around the Fe atoms [Figs. 5(d)–5(f)].

[1] Y. Kamihara, T. Watanabe, M. Hirano, and H. Hosono, J. Am. Chem. Soc. **130**, 3296 (2008).
[2] F.-C. Hsu, J.-Y. Luo, K.-W. Yeh, T.-K. Chen, T.-W. Huang, P. M. Wu, Y.-C. Lee, Y.-L. Huang, Y.-Y. Chu, D.-C. Yan, and M.-K. Wu, Proc. Natl. Acad. Sci. USA **105**, 14262 (2008).
[3] X. C. Wang, Q. Q. Liu, Y. X. Lv, W. B. Gao, L. X. Yang, R. C. Yu, F. Y. Li, and C. Q. Jin, Solid State Commun. **148**, 538 (2008).
[4] M. Rotter, M. Tegel, and D. Johrendt, Phys. Rev. Lett. **101**, 107006 (2008).
[5] H. Takahashi, K. Igawa, K. Arii, Y. Kamihara, M. Hirano, and H. Hosono, Nature (London) **453**, 376 (2008).
[6] X. H. Chen, T. Wu, G. Wu, R. H. Liu, H. Chen, and D. F. Fang, Nature (London) **453**, 761 (2008).
[7] G. F. Chen, Z. Li, D. Wu, G. Li, W. Z. Hu, J. Dong, P. Zheng, J. L. Luo, and N. L. Wang, Phys. Rev. Lett. **100**, 247002 (2008).
[8] J. Paglione and R. L. Greene, Nat. Phys. **6**, 645 (2010).
[9] G. R. Stewart, Rev. Mod. Phys. **83**, 1589 (2011).
[10] T. M. McQueen, A. J. Williams, P. W. Stephens, J. Tao, Y. Zhu, V. Ksenofontov, F. Casper, C. Felser, and R. J. Cava, Phys. Rev. Lett. **103**, 057002 (2009).
[11] P. A. Lee, N. Nagaosa, and X. G. Wen, Rev. Mod. Phys. **78**, 17 (2006).
[12] J. J. Ying, X. F. Wang, X. G. Luo, A. F. Wang, M. Zhang, Y. J. Yan, Z. J. Xiang, R. H. Liu, P. Cheng, G. J. Ye, and X. H. Chen, Phys. Rev. B **83**, 212502 (2011).
[13] J. G. Guo, S. F. Jin, G. Wang, S. C. Wang, K. X. Zhu, T. T. Zhou, M. He, and X. L. Chen, Phys. Rev. B **82**, 180520(R) (2010).
[14] L.-L. Sun, X.-J. Chen, J. Guo, P.-W. Gao, Q.-Z. Huang, H.-D. Wang, M.-H. Fang, X.-L. Chen, G.-F. Chen, Q. Wu, C. Zhang, D.-C. Gu, X.-L. Dong, L. Wang, K. Yang, A.-G. Li, X. Dai, H.-K. Mao, and Z.-X. Zhao, Nature (London) **483**, 67 (2012).
[15] C.-H. Li, B. Shen, F. Han, X. Y. Zhu, and H.-H. Wen, Phys. Rev. B **83**, 184521 (2011).
[16] M.-H. Fang, H.-D. Wang, C.-H. Dong, Z.-J. Li, C.-M. Feng, J. Chen, and H. Q. Yuan, Europhys. Lett. **94**, 27009 (2011).
[17] M. Burrard-Lucas, D. G. Free, S. J. Sedlmaier, J. D. Wright, S. J. Cassidy, Y. Hara, A. J. Corkett, T. Lancaster, P. J. Baker, S. J. Blundell, and S. J. Clarke, Nat. Mater. **12**, 15 (2013).
[18] H.-C. Lei, J.-G. Guo, F. Hayashi, and H. Hosono, Phys. Rev. B **90**, 214508 (2014).
[19] A. Krzton-Maziopa, E. V. Pomjakushina, V. Yu Pomjakushin, F. von Rohr, A. Schilling, and K. Conder, J. Phys.: Condens. Matter **24**, 382202 (2012).
[20] X. F. Lu, N. Z. Wang, H. Wu, Y. P. Wu, D. Zhao, X. Z. Zeng, X. G. Luo, T. Wu, W. Bao, G. H. Zhang, F. Q. Huang, Q. Z. Huang, and X. H. Chen, Nat. Mater. **14**, 325 (2015).
[21] B. Lei, Z. J. Xiang, X. F. Lu, N. Z. Wang, J. R. Chang, C. Shang, A. M. Zhang, Q. M. Zhang, X. G. Luo, T. Wu, Z. Sun, and X. H. Chen, Phys. Rev. B **93**, 060501(R) (2016).
[22] M. Abdel-Hafiez, Y.-Y. Zhang, Z.-Y. Cao, C.-G. Duan, G. Karapetrov, V. M. Pudalov, V. A. Vlasenko, A. V. Sadakov,

D. A. Knyazev, T. A. Romanova, D. A. Chareev, O. S. Volkova, A. N. Vasiliev, and X.-J. Chen, Phys. Rev. B **91**, 165109 (2015).
[23] B. Lei, J. H. Cui, Z. J. Xiang, C. Shang, N. Z. Wang, G. J. Ye, X. G. Luo, T. Wu, Z. Sun, and X. H. Chen, Phys. Rev. Lett. **116**, 077002 (2016).
[24] Q.-Y. Wang, Z. Li, W.-H. Zhang, Z.-C. Zhang, J.-S. Zhang, W. Li, H. Ding, Y.-B. Ou, P. Deng, K. Chang, J. Wen, C.-L. Song, K. He, J.-F. Jia, S.-H. Ji, Y.-Y. Wang, L.-L. Wang, X. Chen, X.-C. Ma, and Q.-K. Xue, Chin. Phys. Lett. **29**, 037402 (2012).
[25] Y. Miyata, K. Nakayama, K. Sugawara, T. Sato, and T. Takahashi, Nat. Mater. **14**, 775 (2015).
[26] C.-J. Tang, D. Zhang, Y.-Y. Zang, C. Liu, G.-Y. Zhou, Z. Li, C. Zheng, X.-P. Hu, C.-L. Song, S.-H. Ji, K. He, X. Chen, L.-L. Wang, X.-C. Ma, and Q.-K. Xue, Phys. Rev. B **92**, 180507(R) (2015).
[27] C. H. P. Wen, H. C. Xu, C. Chen, Z. C. Huang, X. Lou, Y. J. Pu, Q. Song, B. P. Xie, M. Abdel-Hafiez, D. A. Chareev, A. N. Vasiliev, R. Peng, and D. L. Feng, Nat. Commun. **7**, 10840 (2016).
[28] C.-L. Song, H.-M. Zhang, Y. Zhong, X.-P. Hu, S.-H. Ji, L. Wang, K. He, X.-C. Ma, and Q.-K. Xue, Phys. Rev. Lett. **116**, 157001 (2016).
[29] G. Yao, M.-C. Duan, N.-N. Liu, Y.-F. Wu, D.-D. Guan, S.-Y. Wang, H. Zheng, Y.-Y. Li, C.-H. Liu, and J.-F. Jia, Phys. Rev. Lett. **123**, 257001 (2019).
[30] F.-W. Zheng, L.-L. Wang, Q.-K. Xue, and P. Zhang, Phys. Rev. B **93**, 075428 (2016).
[31] G. Kresse and D. Joubert, Phys. Rev. B **59**, 1758 (1999).
[32] P. E. Blöchl, Phys. Rev. B **50**, 17953 (1994).
[33] G. Kresse and J. Furthmüller, Comput. Mater. Sci. **6**, 15 (1996).
[34] G. Kresse and J. Hafner, Phys. Rev. B **47**, 558 (1993).
[35] G. Kresse and J. Furthmüller, Phys. Rev. B **54**, 11169 (1996).
[36] J. P. Perdew, K. Burke, and M. Ernzerhof, Phys. Rev. Lett. **77**, 3865 (1996).
[37] T. M. McQueen, Q. Huang, V. Ksenofontov, C. Felser, Q. Xu, H. Zandbergen, Y. S. Hor, J. Allred, A. J. Williams, D. Qu, J. Checkelsky, N. P. Ong, and R. J. Cava, Phys. Rev. B **79**, 014522 (2009).
[38] X. Wu, M. C. Vargas, S. Nayak, V. Lotrich, and G. Scoles, J. Chem. Phys. **115**, 8748 (2001).
[39] S. Grimme, J. Comput. Chem. **27**, 1787 (2006).
[40] Q.-Q. Ye, K. Liu, and Z.-Y. Lu, Phys. Rev. B **88**, 205130 (2013).
[41] C.-J. Tang, C. Liu, G.-Y. Zhou, F.-S. Li, H. Ding, Z. Li, D. Zhang, Z. Li, C.-L. Song, S.-H. Ji, K. He, L.-L. Wang, X.-C. Ma, and Q.-K. Xue, Phys. Rev. B **93**, 020507(R) (2016).
[42] T.-T. Gai, P.-J. Guo, H.-C. Yang, Y. Gao, M. Gao, and Z.-Y. Lu, Phys. Rev. B **105**, 224514 (2022).
[43] S.-P. Kou, T. Li, and Z.-Y. Weng, Europhys. Lett. **88**, 17010 (2009).
[44] D. Guterding, H. O. Jeschke, P. J. Hirschfeld, and R. Valentí, Phys. Rev. B **91**, 041112(R) (2015).
[45] M. V. Sadovskii, E. Z. Kuchinskii, and I. A. Nekrasov, J. Magn. Magn. Mater. **324**, 3481 (2012).
[46] C. C. Tsuei, C. C. Chi, D. M. Newns, P. C. Pattnaik, and M. Däumling, Phys. Rev. Lett. **69**, 2134 (1992).
[47] S.-L. He, J.-F. He, W.-H. Zhang, L. Zhao, D.-F. Liu, X. Liu, D.-X. Mou, Y.-B. Ou, Q.-Y. Wang, Z. Li, L.-L. Wang, Y.-Y. Peng, Y. Liu, C.-Y. Chen, L. Yu, G.-D. Liu, X.-L. Dong, J. Zhang, C.-T. Chen, Z.-Y. Xu *et al.*, Nat. Mater. **12**, 605 (2013).
[48] N. Li, Z. Li, H. Ding, S.-H. Ji, X. Chen, and Q.-K. Xue, Appl. Phys. Express **6**, 113101 (2013).
[49] W.-H. Zhang, Y. Sun, J.-S. Zhang, F.-S. Li, M.-H. Guo, Y.-F. Zhao, H.-M. Zhang, J.-P. Peng, Y. Xing, H.-C. Wang, T. Fujita, A. Hirata, Z. Li, H. Ding, C.-J. Tang, M. Wang, Q.-Y. Wang, K. He, S.-H. Ji, X. Chen *et al.*, Chin. Phys. Lett. **31**, 017401 (2014).
[50] Z. Li, J.-P. Peng, H.-M. Zhang, W.-H. Zhang, H. Ding, P. Deng, K. Chang, C.-L. Song, S.-H. Ji, L.-L. Wang, K. He, X. Chen, Q.-K. Xue, and X.-C. Ma, J. Phys.: Condens. Matter **26**, 265002 (2014).
[51] W.-H. Zhang, Z. Li, F.-S. Li, H.-M. Zhang, J.-P. Peng, C.-J. Tang, Q.-Y. Wang, K. He, X. Chen, L.-L. Wang, X.-C. Ma, and Q.-K. Xue, Phys. Rev. B **89**, 060506(R) (2014).
[52] A. K. Pedersen, S. Ichinokura, T. Tanaka, R. Shimizu, T. Hitosugi, and T. Hirahara, Phys. Rev. Lett. **124**, 227002 (2020).
[53] S.-Y. Tan, Y. Zhang, M. Xia, Z.-R. Ye, F. Chen, X. Xie, R. Peng, D.-F. Xu, Q. Fan, H.-C. Xu, J. Jiang, T. Zhang, X.-C. Lai, T. Xiang, J.-P. Hu, B.-P. Xie, and D.-L. Feng, Nat. Mater. **12**, 634 (2013).
[54] Y.-Y. Xiang, F. Wang, D. Wang, Q.-H. Wang, and D.-H. Lee, Phys. Rev. B **86**, 134508 (2012).
[55] S. Coh, M. L. Cohen, and S. G. Louie, New J. Phys. **17**, 073027 (2015).
[56] K. Liu, B.-J. Zhang, and Z.-Y. Lu, Phys. Rev. B **91**, 045107 (2015).
[57] Z.-X. Li, F. Wang, H. Yao, and D.-H. Lee, Sci. Bull. **61**, 925 (2016).
[58] Z.-X. Li, T. P. Devereaux, and D.-H. Lee, Phys. Rev. B **100**, 241101(R) (2019).
[59] F. Yang, F. Wang, and D.-H. Lee, Phys. Rev. B **88**, 100504(R) (2013).
[60] V. Savinov, Novel toroidal and superconducting metamaterials, Ph.D. thesis, University of Southampton, 2014, p. 64.
[61] T. Onimaru, K. T. Matsumoto, Y. F. Inoue, K. Umeo, T. Sakakibara, Y. Karaki, M. Kubota, and T. Takabatake, Phys. Rev. Lett. **106**, 177001 (2011).
[62] K. Matsubayashi, T. Tanaka, A. Sakai, S. Nakatsuji, Y. Kubo, and Y. Uwatoko, Phys. Rev. Lett. **109**, 187004 (2012).
[63] M. Tsujimoto, Y. Matsumoto, T. Tomita, A. Sakai, and S. Nakatsuji, Phys. Rev. Lett. **113**, 267001 (2014).
[64] S. Sumita and Y. Yanase, Phys. Rev. Res. **2**, 033225 (2020).